Journal of Power Sources 226 (2013) 354–358

Contents lists available at SciVerse ScienceDirect

Journal of Power Sources

journal homepage: www.elsevier.com/locate/jpowsour

Short communication

High performance of $La_{0.6}Sr_{0.4}Co_{0.2}Fe_{0.8}O_3$–$Ce_{0.9}Gd_{0.1}O_{1.95}$ nanoparticulate cathode for intermediate temperature microtubular solid oxide fuel cells

Hirofumi Sumi*, Toshiaki Yamaguchi, Koichi Hamamoto, Toshio Suzuki, Yoshinobu Fujishiro

Advanced Manufacturing Research Institute, National Institute of Advanced Industrial Science and Technology, Nagoya 463-8560, Japan

HIGHLIGHTS

- Grain size of LSCF–GDC nanoparticulate cathode was less than 100 nm.
- Total cathode polarization resistance was only 0.13 Ω cm^2 at 600 °C.
- LSCF nanoparticulate cathode contributed to decrease the polarization resistance.

GRAPHICAL ABSTRACT

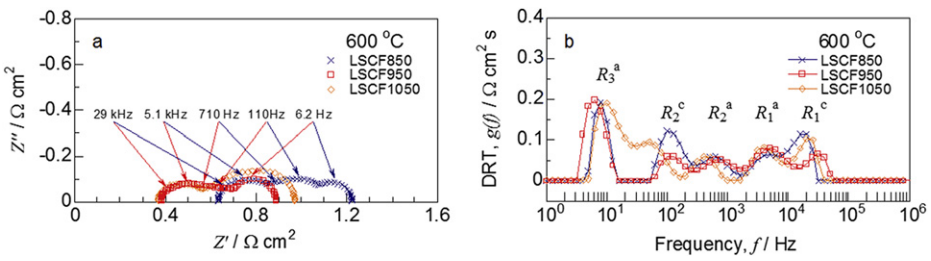

ARTICLE INFO

Article history:
Received 20 August 2012
Received in revised form
5 November 2012
Accepted 8 November 2012
Available online 16 November 2012

Keywords:
Solid oxide fuel cell (SOFC)
Perovskite
Cathode
AC impedance
Distribution of relaxation times (DRT)

ABSTRACT

The perovskite $La_{0.6}Sr_{0.4}Co_{0.2}Fe_{0.8}O_3$–$Ce_{0.9}Gd_{0.1}O_{1.95}$ (LSCF–GDC) nanoparticulate cathode was applied for microtubular solid oxide fuel cells operated at intermediate temperatures. For the cell with the cathode sintered at 950 °C, maximum power densities of 0.26, 0.54 and 0.73 W cm^{-2} were obtained at 550, 600 and 650 °C, respectively. The ohmic resistance increased for the cathode sintered at 850 °C, and the polarization resistance increased for the cathode sintered at 1050 °C. The cathode polarization resistances of ionic conduction process in the LSCF bulk and adsorption/desorption process on the LSCF surface were estimated by the distribution of relaxation times analysis, which were only 0.066 and 0.065 Ω cm^2 at 600 °C for the cathode sintered at 950 °C. The grain size of the cathode was less than 100 nm, which resulted in high performance due to an overall decrease in cathode polarization resistance.

© 2012 Elsevier B.V. All rights reserved.

1. Introduction

Solid oxide fuel cells (SOFCs) are expected to emerge as power generation systems with high energy conversion efficiencies. Recently, many researchers have focused on lowering the operating temperature of SOFCs from 800–1000 °C to 500–700 °C in order to improve their durability, start-up time and so on. Previously, the authors have developed anode-supported microtubular SOFCs with high power densities via the "Advanced Ceramic Reactor Project" of the New Energy and Industrial Technology Development Organization (NEDO) in Japan. We have successfully formed dense electrolyte thin-films of thickness *ca.* 5 μm by dip-coating on the anode substrate, which contributes to a decrease in the ohmic resistance [1]. The anode polarization resistance is decreased by controlling the nanostructure of the anode substrate using acrylic resin as a pore former [2]. The power density per cathode area reached 1 W cm^{-2} at a low temperature of 550 °C for the microtubular SOFCs with a diameter of 0.8 mm [3]. Furthermore, a power of 2 W can be obtained at 490 °C for a 3 × 3-cell module with a volume of 1 cm^3 [4].

High catalytic and electrochemical activities are also required to promote oxide ion transfer and oxygen exchange processes as well

* Corresponding author. Tel.: +81 52 736 7592; fax: +81 52 736 7405.
E-mail address: h-sumi@aist.go.jp (H. Sumi).

0378-7753/$ – see front matter © 2012 Elsevier B.V. All rights reserved.
http://dx.doi.org/10.1016/j.jpowsour.2012.11.015

as high electronic conductivities at low temperatures for cathode materials. Perovskite $La_{0.6}Sr_{0.4}Co_{0.2}Fe_{0.8}O_3$ (LSCF) is one of the most promising cathodes for intermediate temperature (IT)-SOFCs. The LSCF cathode is a mixed ionic–electronic conductor with an electrical conductivity of more than 10^2 S cm^{-1} at 500–700 °C, and is a good match with zirconia based electrolytes in terms of its thermal expansion coefficient [5,6]. Dusastre and Kilner [7] and Murray et al. [8] reported that the cathode polarization resistance decreased significantly by adding 30–50 vol.% Gd-doped ceria (GDC) to LSCF. Furthermore, the adding of a noble metal catalyst such as Pd [9], Pt [10], Ag [11] and so on into LSCF promoted the cathode reaction at temperatures below 600 °C. However, the noble catalysts are too expensive to be applied to IT-SOFCs. Recently, Shah and Barnett [12], Darbandi and Hahn [13] and Leng et al. [14] developed nanoparticulate cathodes with high catalytic and electrochemical activities for IT-SOFCs. They only evaluated half-cells in air to investigate cathode polarization resistance using an AC impedance method.

Previously, the authors were successful in evaluating the effect of anode porosity on the polarization resistance by the distribution of relaxation times (DRT) analysis [15]. This method can directly detect the number of electrode processes using mathematical techniques without assuming the equivalent circuits for actual SOFCs in hydrogen/air [16,17]. In this study, the polarization resistances of the LSCF–GDC nanoparticulate cathodes with different sintering temperatures were evaluated by the DRT analysis for anode-supported microtubular SOFCs.

2. Experimental

Anode microtubes were made from NiO (Sumitomo metal mining), 8 mol% Y_2O_3 stabilized ZrO_2 (8YSZ; Tosoh), pore former (acrylic resin; Sekisui Plastic) and binder (Cellulose; Yuken Kogyo) powders. The weight ratio of NiO to 8YSZ was 60:40, and the particle size of the pore former was *ca.* 5 μm. These powders were mixed with a kneading machine by adding an appropriate amount of water over a period of 2 h. The hardness of the mixture clay was *ca.* 12 measured by a type A durometer (ISO 7619). The anode microtubes were extruded using a piston cylinder with a metal hold with an outside diameter of 2.4 mm and an inside diameter of 2.0 mm. After extrusion, the tubes were dried overnight in air at room temperature. A slurry was prepared by mixing 8YSZ, binder (polyvinyl butyral; Sekisui Chemical) dispersant (tallow propylene diamine, Kao) and plasticizer (dioctyl adipate; Wako Pure Chemical Industries) into ethanol and toluene solvents for 48 h. The 8YSZ electrolyte was formed by dip-coating at a pulling rate of 1 mm s^{-1}. The 8YSZ thin-film electrolyte and NiO-8YSZ anode microtube were co-sintered for 1 h in air at 1350 °C. The interlayer of $Ce_{0.9}Gd_{0.1}O_{1.95}$ (GDC; Shin-etsu Chemical) was formed on the electrolyte by a similar manner, and sintered for 1 h in air at 1200 °C. The cathode was a LSCF–GDC (70:30 wt.%) composite. The LSCF nanoparticulate powder was prepared using co-precipitation and low temperature calcination by Dowa Electronics Materials. The LSCF–GDC cathode was formed by dip-coating at a pulling rate of 2 mm s^{-1}, and sintered for 1 h in air at 850, 950 or 1050 °C (denoted LSCF850–GDC, LSCF950–GDC and LSCF1050–GDC, respectively). The outside diameter of the microtubes was 1.8 mm and the area of the cathode was 0.6 cm^2 after sintering. The thicknesses of the anode, the electrolyte, the interlayer and the cathode were *ca.* 200, 5, 1 and 20 μm, respectively. The cathode microstructure was observed using a FE-SEM (JEOL; JSM-6330F) with an accelerating voltage of 15 kV.

The characteristics of the power generation and the AC impedance were evaluated with a potentiostat/galvanostat (Solartron Analytical 1287) and an impedance analyzer (Solartron Analytical 1255B). A mixture of 40% H_2–3% H_2O–57% N_2 was supplied as fuel at a flow rate of 50 mL min^{-1} to the anode side, and air was supplied as oxidant at 50 mL min^{-1} to the cathode side. Operating temperatures were 500, 550, 600 and 650 °C. Silver wires were used as current collectors. Current–potential (i–V) characteristics were measured from open circuit voltage (OCV) to 0.4 V at a sweep rate of 5 mV s^{-1}. AC impedance spectra were measured under OCV in the frequency range from 1 MHz to 0.1 Hz with 20 steps per logarithmic decade.

Generally, polarization resistances are analyzed by an equivalent circuit with a parallel resistance–conductance (RC) element. An ideal RC element has a single relaxation time τ defined by the appropriate R and C values ($\tau = RC$). However, the actual polarization resistance for SOFCs cannot be perfectly fitted by one RC element because relaxation times are generally distributed for the actual electrode processes. Therefore, the polarization resistances are generally fitted by an equivalent circuit with RQ element (constant phase elements in parallel with a resistor) for the complex non-linear least squares (CNLS) method [18]. The DRT method can directly detect the number of electrode processes by mathematical techniques without assuming the equivalent circuits of the polarization components [16,17]. In this study, polarization impedance $Z_{pol}(\omega)$ are considered to be an equivalent circuit composed of an infinite number of RC elements in the following series.

$$Z_{pol}(\omega) = R_{pol}\int_0^\infty \frac{\gamma(\tau)}{1+j\omega\tau}d\tau \quad \text{with} \quad \int_0^\infty \gamma(\tau)d\tau = 1 \tag{1}$$

here, R_{pol} is the total DC polarization resistance, $\gamma(\tau)$ is the DRT, ω is the angular frequency and j is the imaginary unit. The distribution function $g(f)$ (with $f = \omega/2\pi$) was calculated using the software program FTIKREG [19] to solve an ill-posed inverse problem by Tikhonov regularization. However, it was impossible to obtain good results for DRT analysis for impedance spectra with an inductance at high frequency [15]. The inductance components were removed by the same method as described in Ref. [15] before DRT analysis for the impedance spectra in this study.

3. Results and discussion

Fig. 1 shows the scanning electron images of the (a) LSCF850–GDC, (b) LSCF950–GDC and (c) LSCF1050–GDC cathodes after sintering. The LSCF nanoparticulate powder can be obtained by co-precipitation and low temperature calcination. The grain size of the LSCF850–GDC was only 30–50 nm as shown in Fig. 1(a). The LSCF grains grew up when the sintering temperatures were increased. The size of LSCF1050 was approximately 100 nm. Furthermore, grains more than 300 nm in diameter were observed after sintering at 1050 °C. They are likely to be GDC, because the GDC grains were further grown to a diameter of *ca.* 1 μm in the interlayer sintered at 1200 °C as shown in the lower image of Fig. 1. The grain size is expected to affect the length of double phase boundaries and electronic conduction paths. On the other hand, the electrolyte and the interlayer were in good contact for all of the cathodes. However, the interface between interlayer and the cathode was unclear because the both of the layers were porous. It was expected that the cathode sintered at the higher temperature was in better contact between the interlayer and the cathode.

Fig. 2 shows the i–V characteristics for the anode-supported microtubular SOFCs with the LSCF850–GDC, LSCF950–GDC and LSCF1050–GDC cathodes at 500–650 °C. Regarding the influence of the sintering temperature, the electrode sintered at 950 °C gave the best performance. At an operating temperature of 600 °C, the maximum power densities were 0.41, 0.54 and 0.49 W cm^{-2}, and the area specific resistances (ASRs) derived from the slopes of the i–V curves near OCV were 1.2, 0.88 and 0.94 Ω cm^2 for the

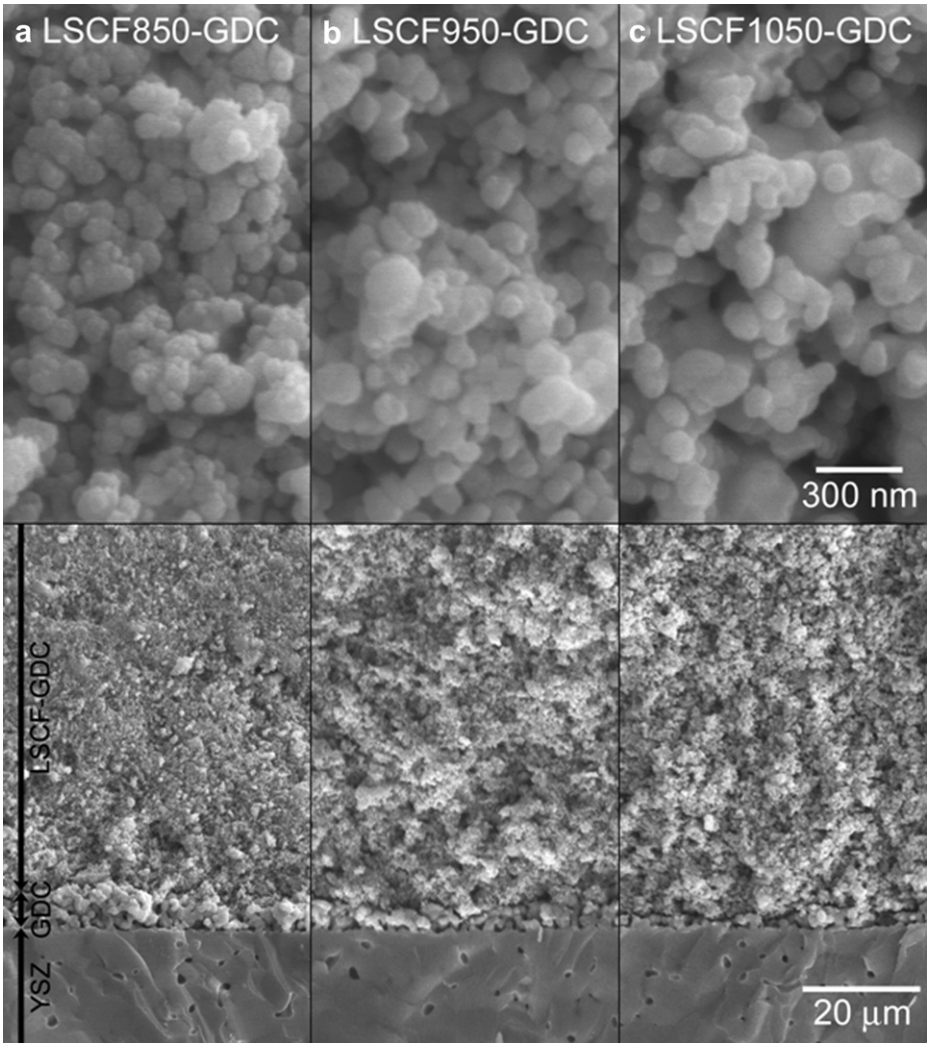

Fig. 1. Scanning electron images of (a) LSCF850–GDC, (b) LSCF950–GDC and (c) LSCF1050–GDC cathodes after sintering.

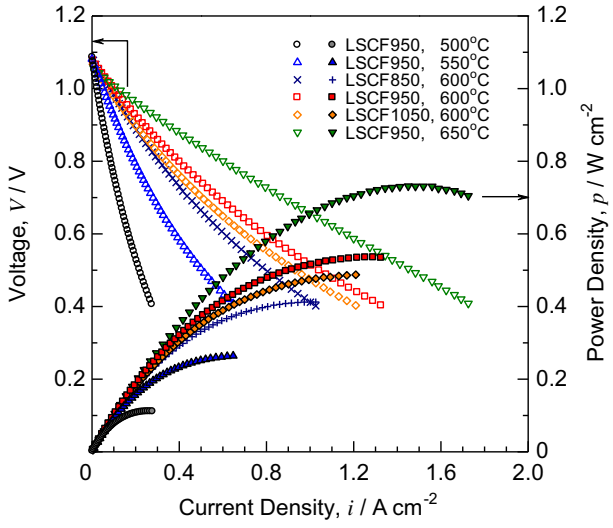

Fig. 2. Current–potential characteristics for anode-supported microtubular SOFCs with LSCF850–GDC, LSCF950–GDC and LSCF1050–GDC cathodes at 500–650 °C. The fuel was 40% H_2–3% H_2O–57% N_2 mixture, and the oxidant was air. The flow rate was 50 mL min^{-1}.

LSCF850–GDC, LSCF950–GDC and LSCF1050–GDC cathodes, respectively. This result suggests that the optimum sintering temperature is 950 °C for the LSCF nanoparticulate cathode in this study. The cell performance was improved by the increase in operating temperature. The maximum power density reached 0.73 W cm^{-2} at 650 °C for the LSCF950–GDC cathode. Furthermore, the power density of 0.26 W cm^{-2} was able to be obtained even at a temperature as low as 550 °C. This is confirmed to be an advantage of the LSCF nanoparticulate cathode at low operating temperatures.

We measured and analyzed the AC impedance precisely for the anode-supported SOFCs with the LSCF nanoparticulate cathodes. Fig. 3(a) shows the impedance spectra for the cells with the LSCF950–GDC cathode at 500–650 °C. The AC impedances were measured under OCV. Both the ohmic and polarization resistances decreased with a rise in operating temperature. The total resistances evaluated by AC impedance agreed well with the ASRs derived from the slopes of the i–V curves near the OCV in Fig. 2. The ohmic resistances at 500, 550, 600 and 650 °C were 1.3, 0.68, 0.38 and 0.23 Ω cm^2 for the whole cell with the LSCF950–GDC cathode. Fig. 3(b) shows the impedance spectra for the cells with the LSCF850–GDC, LSCF950–GDC and LSCF1050–GDC cathodes at 600 °C. The ohmic and polarization resistances were minimal for the LSCF950–GDC cathode. The ohmic resistance for the LSCF850–

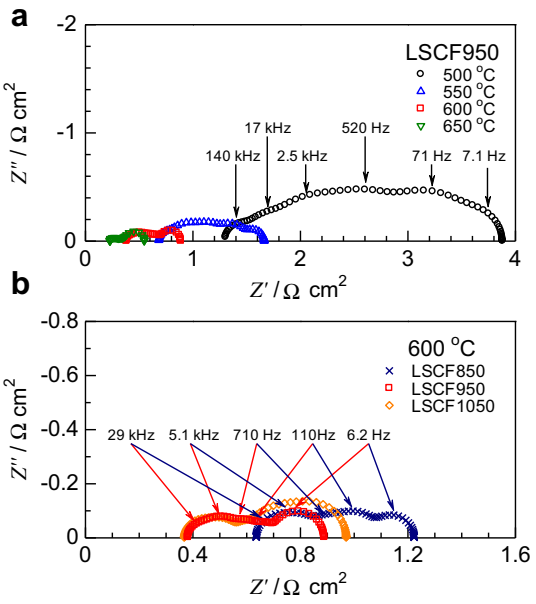

Fig. 3. AC impedance spectra for anode-supported microtubular SOFCs (a) with LSCF950–GDC cathode at 500–650 °C, and (b) with LSCF850–GDC, LSCF950–GDC and LSCF1050–GDC cathodes at 600 °C. The impedances were measured between anode and cathode under OCV state.

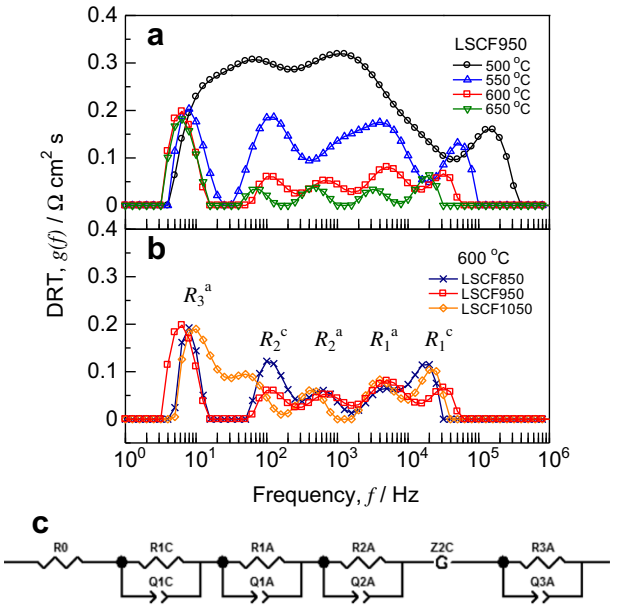

Fig. 4. DRT spectra for anode-supported microtubular SOFCs (a) with LSCF950–GDC cathode at 500–650 °C, (b) with LSCF850–GDC, LSCF950–GDC and LSCF1050–GDC cathodes at 600 °C, and (c) equivalent circuit for CLNS fitting to estimate the ohmic and polarization resistances.

GDC cathode was larger than that for the other cathodes. This result supported the hypothesis that sintering the LSCF–GDC nanoparticulate cathode at low temperatures causes poor electronic conduction paths in the cathode and/or poor contact areas between the cathode and the interlayer. The total polarization resistance also increased under the influence of high ohmic resistance for the LSCF850–GDC cathode. On the other hand, the polarization resistances became large for the LSCF1050–GDC cathode. The semicircle around 110 Hz especially increased in comparison with the LSCF950–GDC cathode, which was likely caused by the decrease in double phase boundaries in the cathode sintered at temperatures as high as 1050 °C. However, it is too difficult to discuss the polarization resistances precisely, because several semicircles overlapped in the Nyquist plots given in Fig. 3.

The DRT analysis was applied to separate each polarization resistance for the anode-supported microtubular SOFCs in this study. Fig. 4(a) shows the DRT spectra for the cells with the LSCF950–GDC cathode at 500–650 °C. Five peaks were detected by the DRT analysis, which agreed with the previous report [15]. The peaks at the lowest frequency (R_3^a) changed only slightly with respect to the operating temperature. It was previously confirmed that this peak was ascribed to the anode diffusion resistance, and its activation energy was small for the anode-supported microtubular SOFCs [15]. The other polarization resistances decreased as the operating temperature was increased. The peaks of R_1^a and R_2^a were ascribed to anode activation resistances confirmed in the previous report [15]. On the other hand, Koyama et al. suggested that the rate-determining steps of cathode reaction were (i) the ionic conduction in the mixed ionic–electronic conductor and (ii) the adsorption/desorption process on the surface of the electrode [20]. The (i) and (ii) occur at ≥1 kHz and ~10 Hz [21,22], which corresponds to R_1^c and R_2^c, respectively, for the DRT spectra as shown in Fig. 4. For precise discussion, of course, we should investigate the oxygen partial pressure (p_{O_2}) dependence of cathode polarization resistances. The polarization resistance of surface process is theoretically proportional to $p_{O_2}^{-1/2}$ [20,23]. On the other hand, Baek et al. confirmed experimentally that the p_{O_2} dependence of R_1^c was *ca.* −0.25 power, which was ascribed to ionic conduction in $Sm_{0.5}Sr_{0.5}Co_{3-\delta}$–$Sm_{0.2}Ce_{0.8}O_{1.9}$ cathode [24]. Fig. 4(b) shows the DRT spectra for the LSCF850–GDC, LSCF950–GDC and LSCF1050–GDC cathodes at 600 °C. The anode polarization resistances (R_1^a, R_2^a and R_3^a) were nearly the same for all samples at 600 °C. The cathode polarization resistance (R_1^c and R_2^c) for the LSCF950–GDC was the smallest when compared to the other cathodes. The values of polarization resistances are summarized in Table 1 derived from the DRT analysis and CNLS fitting in consideration of Gerischer impedance as shown in Fig. 4(c) [21,22,25].

$$Z_2^c(\omega) = \frac{R_2^c}{\sqrt{1 + j\omega\tau_2^c}} \tag{2}$$

The LSCF850–GDC cathode had a large ohmic resistance as shown in Fig. 3(b), which also affected the increase in the polarization resistance. For LSCF1050–GDC cathode, the GDC grains have grown up significantly as shown in Fig. 1(c). The polarization resistance increased by the decrease in the double phase boundary of LSCF/GDC sintered at 1050 °C. On the other hand, the grain

Table 1
The polarization resistance (Ω cm^2) derived from the DRT analysis for anode-supported microtubular SOFCs with LSCF850–GDC, LSCF950–GDC and LSCF1050–GDC cathodes at 600 °C in comparison with the total cathode polarization resistances in Refs. [7,8,12,13].

	R_1^c	R_2^c	R_1^a	R_2^a	R_3^a
Frequency (Hz)	2.9×10^4	1.1×10^2	5.1×10^3	7.1×10^2	6.2
LSCF850–GDC	0.11	0.15	0.088	0.082	0.16
LSCF950–GDC	0.066	0.065	0.10	0.088	0.18
LSCF1050–GDC	0.094	0.14	0.096	0.065	0.20
Dusastre and Kilner [7]	0.60		–	–	–
Murray et al. [8]	0.33		–	–	–
Shah and Barnett [12]	0.24		–	–	–
Darbandi and Hahn [13]	0.37		–	–	–

growth was relatively suppressed for the LSCF950–GDC cathode as shown in Fig. 1(b), which realized good performance for ionic conduction process in the LSCF bulk and adsorption/desorption process on the LSCF surface. The sum of R_1^c and R_2^c in this study was smaller than the cathode polarization resistances reported in the previous papers [7,8,12,13]. It is concluded that the LSCF–GDC nanoparticulate cathodes can contribute to improve cell performance by decreasing in the polarization resistance.

4. Conclusion

In this study, we evaluated the polarization resistances of the LSCF–GDC nanoparticulate cathodes for anode-supported microtubular SOFCs by DRT analysis. The maximum power densities were 0.26, 0.54 and 0.73 W cm^{-2} for cells with LSCF950–GDC at 550, 600 and 650 °C, respectively. The ohmic resistance increased for the LSCF850–GDC cathode, and the cathode polarization resistance increased for the LSCF1050–GDC cathode. The DRT peaks at *ca.* 10 kHz and 10 Hz changed by the sintering temperature of the LSCF–GDC cathode. The cathode polarization resistances of ionic conduction process in the LSCF bulk and adsorption/desorption process on the LSCF surface were only 0.066 and 0.065 Ω cm^2 for the LSCF950–GDC cathode at 600 °C. The LSCF–GDC nanoparticulate cathode with a grain size of less than 100 nm can realize high performance by the decrease in the polarization resistance for IT-SOFCs.

Acknowledgment

The LSCF nanoparticulate powders were provided by Dowa Electronics Materials Co., Ltd. The authors would like to express thanks to Professor Toshiaki Matsui and Professor Koichi Eguchi, Kyoto University, for their valuable advice regarding DRT analysis.

References

[1] T. Suzuki, T. Yamaguchi, Y. Fujishiro, M. Awano, J. Electrochem. Soc. 153 (2006) A925.
[2] T. Suzuki, Z. Hasan, Y. Funahashi, T. Yamaguchi, Y. Fujishiro, M. Awano, Science 325 (2009) 852.
[3] T. Suzuki, Y. Funahashi, T. Yamaguchi, Y. Fujishiro, M. Awano, Electrochem. Solid State Lett. 10 (2007) A177.
[4] T. Suzuki, Y. Funahashi, T. Yamaguchi, Y. Fujishiro, M. Awano, J. Power Sources 183 (2008) 544.
[5] L.-W. Tai, M.M. Nasrallah, H.U. Anderson, D.M. Sparlin, S.R. Sehlin, Solid State Ionics 76 (1995) 259.
[6] L.-W. Tai, M.M. Nasrallah, H.U. Anderson, D.M. Sparlin, S.R. Sehlin, Solid State Ionics 76 (1995) 273.
[7] V. Dusastre, J.A. Kilner, Solid State Ionics 126 (1999) 163.
[8] E.P. Murray, M.J. Sever, S.A. Barnett, Solid State Ionics 148 (2002) 27.
[9] M. Sahibzada, S.J. Benson, R.A. Rudkin, J.A. Kilner, Solid State Ionics 113–115 (1998) 285.
[10] H.J. Hwang, J.W. Moon, S. Lee, E.A. Lee, J. Power Sources 145 (2005) 243.
[11] T. Suzuki, P. Jasinski, H.U. Anderson, F. Dogan, J. Electrochem. Soc. 151 (2004) A1678.
[12] M. Shah, S.A. Barnett, Solid State Ionics 179 (2008) 2059.
[13] A.J. Darbandi, H. Hahn, Solid State Ionics 180 (2009) 1379.
[14] Y. Leng, S.H. Chan, Q. Liu, Int. J. Hydrogen Energ. 33 (2008) 3808.
[15] H. Sumi, T. Yamaguchi, K. Hamamoto, T. Suzuki, Y. Fujishiro, Electrochim. Acta 67 (2012) 159.
[16] H. Schichlein, A.C. Müller, M. Voigts, A. Krügel, E. Ivers-Tiffée, J. Appl. Electrochem. 32 (2002) 875.
[17] A. Leonide, V. Sonn, A. Weber, E. Ivers-Tiffée, J. Electrochem. Soc. 155 (2008) B36.
[18] J.R. Macdonald, Impedance Spectroscopy, Wiley Interscience, New York, 1987.
[19] J. Weese, Comput. Phys. Commun. 69 (1992) 99.
[20] M. Koyama, C.-J. Wen, T. Masuyama, J. Otomo, H. Fukunaga, K. Yamada, K. Eguchi, H. Takahashi, J. Electrochem. Soc. 148 (2001) A795.
[21] S.B. Adler, J.A. Lane, B.C.H. Steele, J. Electrochem. Soc. 143 (1996) 3554.
[22] S.B. Adler, Solid State Ionics 111 (1998) 125.
[23] Y. Takeda, R. Kanno, M. Noda, Y. Tomida, O. Yamamoto, J. Electrochem. Soc. 134 (1987) 2656.
[24] S.-W. Baek, J. Bae, Y.-S. Yoo, J. Power Sources 193 (2009) 431.
[25] A. Leonide, B. Rüger, A. Weber, W.A. Meulengerg, E. Ivers-Tiffée, J. Electrochem. Soc. 157 (2010) B234.